frontiers in Materials

ORIGINAL RESEARCH
published: 21 September 2020
doi: 10.3389/fmats.2020.567031

An A-π-D-π-A-Type Organic Semiconductor Based Optoelectrical Device With Photo Response and Optical Memory Behaviors

Shiyu Feng[1]*, *Donghuan Dai*[1,2], *Yao Lin*[1], *Shuo Chen*[1,2], *Xiaosong Wu*[1,2] and *Weiguo Huang*[1]*

[1] State Key Laboratory of Structural Chemistry, Fujian Institute of Research on the Structure of Matter, Chinese Academy of Sciences, Fuzhou, China, [2] College of Chemistry and Materials Science, Fujian Normal University, Fuzhou, China

A novel photoactive semiconductor (named as IDTOT-4F) with an A-π-D-π-A-type configuration is synthesized. It contains an electron-donating fused ring (D) as the core flanked with two π-spacers and is end-capped with two electron-withdrawing units (A). The intramolecular charge transfer effect endows IDTOT-4F with strong and broad light absorption and a relatively narrow band gap (1.46 eV). Thin-film optoelectrical devices based on IDTOT-4F exhibit both *n*-type and *p*-type switching behaviors. Besides, the *p*-channel device shows significantly photoresponsive performance with the maximum *P* (photo/dark current ratio), *R* (photoresponsivity), and *D** (detectivity) values of around 60, 0.07 A W^{-1}, and 2.5 × 10^{10} Jones, respectively. Further, IDTOT-4F based optoelectrical devices exhibit good optical memory characteristics with a time constant τ_1 of 4.6 h, indicating its applicability to nonvolatile optical memory devices. The results provide new insights into the photoresponsive behavior of fused-ring semiconductors and pave the way for the design of nonvolatile optical memory devices.

Keywords: photo response, optical memory, A-π-D-π-A-type, photoactive semiconductor, optoelectrical device

OPEN ACCESS

Edited by:
Tao Li,
Shanghai Jiao Tong University, China

Reviewed by:
Xiaotao Zhang,
Tianjin University, China
Yunlong Guo,
Institute of Chemistry (CAS), China

***Correspondence:**
Shiyu Feng
fengshiyu@fjirsm.ac.cn
Weiguo Huang
whuang@fjirsm.ac.cn

Specialty section:
This article was submitted to Energy Materials, a section of the journal Frontiers in Materials

Received: *29 May 2020*
Accepted: *28 August 2020*
Published: *21 September 2020*

Citation:
Feng S, Dai D, Lin Y, Chen S, Wu X and Huang W (2020) An A-π-D-π-A-Type Organic Semiconductor Based Optoelectrical Device With Photo Response and Optical Memory Behaviors. Front. Mater. 7:567031. doi: 10.3389/fmats.2020.567031

INTRODUCTION

Organic photoresponsive semiconductors have drawn tremendous attentions as an exciting candidate for photodetectors (de Arquer et al., 2017; Park et al., 2018; Li et al., 2019; Huang et al., 2020), artificial synaptic devices (Park and Lee, 2017; Dai et al., 2019; Deng et al., 2019; Yu et al., 2019; Shi et al., 2020), and particularly nonvolatile memory (Leydecker et al., 2016; Cheng et al., 2018; Liu et al., 2019; Yu et al., 2019), owing to their facile structure modification, excellent optoelectronic properties, large scale fabrication, low temperature processing, and mechanical flexibility. However, the number of semiconductors with good intrinsic optical memory behavior is small, and systematic studies on the photoresponsive semiconductors are desired. In recent years, A-π-D-π-A-type fused ring semiconductors have been widely used as non-fullerene acceptors in organic solar cells because of their wide spectral response ranging from visible region to near-infrared region, narrow band gaps, and high absorption coefficients (Yao et al., 2017; Hou et al., 2018; Liu et al., 2018; Yan et al., 2018). Relying on these unique optical properties, it is believed that these A-π-D-π-A-type fused ring acceptors would be ideal candidates for organic photodetectors, near-infrared (NIR) image sensors, and even optical memory devices (Lee et al., 2019; Huang et al., 2020). Notably, compared with the A-D-A-type structure, the π-spacer in the A-π-D-π-A-type structure can expand the effective conjugation length of acceptors and further extend their absorptions (Li et al., 2020). To date,

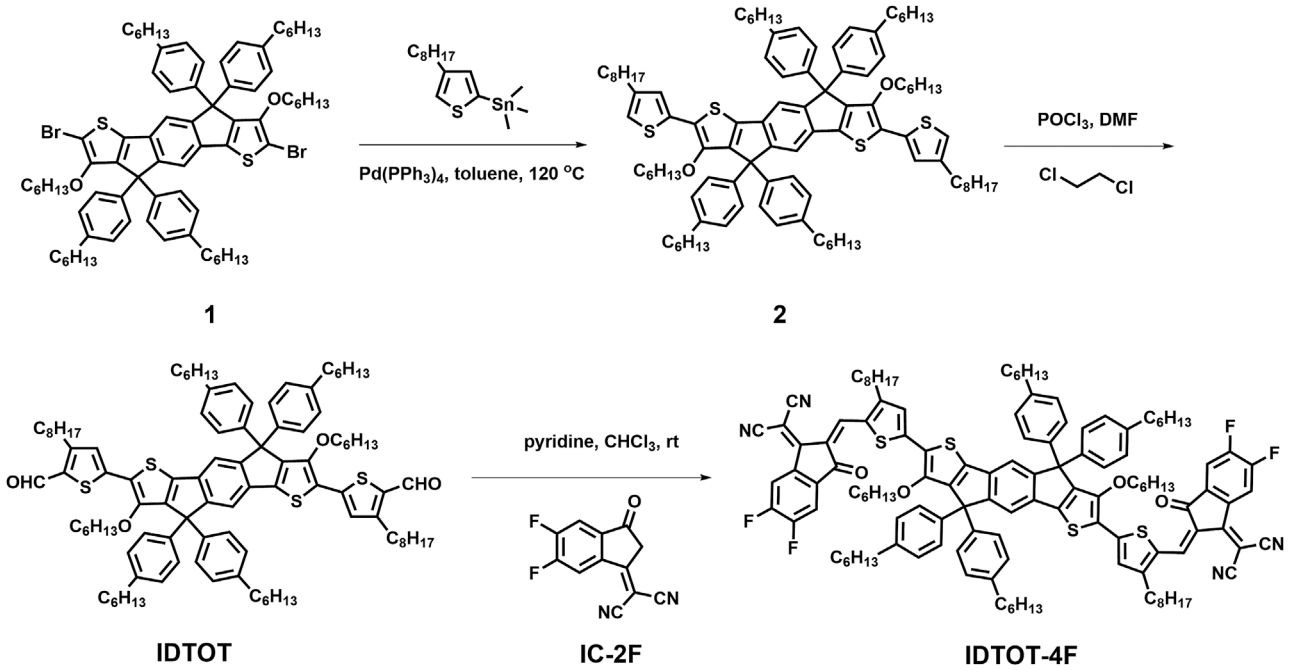

Scheme 1 | Synthetic route of IDTOT-4F.

systematic studies on the photoresponsive behaviors of these A-π-D-π-A-type acceptors are scarce, which might hamper their application on the light stimuli response electronic devices.

In this work, we synthesize a new A-π-D-π-A-type small molecule named as IDTOT-4F and systematically study the photoresponse of devices based on IDTOT-4F. IDTOT-4F uses indacenodithiophene as the central electron-donor unit, which is flanked with two thienyl units as the π-spacers and terminated with 2-(5,6-difluoro-3-oxo-2,3-dihydro-1*H*-inden-1-ylidene) malononitrile (IC-2F) as the electron-acceptor unit. As expected, IDTOT-4F possesses a high molar extinction coefficient of $2.51 \times 10^5\ M^{-1}\ cm^{-1}$, a broad absorption band ranging from 550 to 850 nm, and a narrow band gap of 1.46 eV. Interestingly, IDTOT-4F based devices exhibit both *n*-type and *p*-type switching behaviors, and the *p*-channel device based on IDTOT-4F shows good photoresponse properties. Upon white light irradiation ($4{,}200\ \mu W\ cm^{-2}$) for 10 sec, the *p*-type optoelectrical device raises the saturated I_d from around 100 nA to 1.14 μA ($V_g = V_d = -100$ V) with the photo/dark current ratio (*P*) of 60, photoresponsivity (*R*) of $0.07\ A\ W^{-1}$, and detectivity (D^*) of 2.5×10^{10} Jones. The light intensity and pulse width could promote the photogenerated charge carriers, thus leading to enhanced photoresponsive behaviors and higher hole mobilities. More importantly, IDTOT-4F based optoelectrical devices exhibit good photocurrent memory characteristics with a time constant τ_1 of 4.6 h, indicating its applicability to nonvolatile optical memory devices. The results provide new insights into the photoresponsive behavior of fused-ring semiconductors and pave the way for the design of nonvolatile optical memory devices.

MATERIALS AND METHODS

Material Synthesis

The synthetic route of IDTOT-4F is outlined in **Scheme 1**.

Compound 2

Compound 1 (500 mg, 0.40 mmol), which was synthesized following the reported literature (Liu et al., 2018), and trimethyl (4-octylthiophen-2-yl)stannane (320 mg, 0.89 mmol) were dissolved in anhydrous toluene (20 ml). The mixture was deoxygenated with nitrogen for 10 min before and after adding the catalyst $Pd(PPh_3)_4$ (23 mg, 0.02 mmol) to the solution, and then stirred at 120°C for 48 h. After cooling down to room temperature, the solvent was evaporated, and the resulting mixture was purified by silica gel column chromatography with petroleum ether as the eluent, affording a yellow solid (515 mg, 86%). ^{1}H NMR (500M, $CDCl_3$, δ): 7.26 (s, 2H) overlapping 7.26 ($C\underline{H}Cl_3$), 7.25 (d, J = 8.2 Hz, 8H), 7.06 (d, J = 8.3 Hz, 8H), 7.04 (s, 2H), 6.79 (s, 2H), 3.17 (t, J = 7.0 Hz, 4H), 2.56 (t, J = 7.75 Hz, 12H), 1.63–1.56 (m, 12H), 1.48–1.42 (m, 4H), 1.32–1.26 (m, 44H), 1.25–1.19 (m, 4H), 1.14–1.02 (m, 8H), 0.89–0.83 (m, 24H). ^{13}C (125M, $CDCl_3$, δ): 154.88, 148.89, 143.28, 141.51, 139.84, 137.25, 135.13, 135.01, 128.58, 128.10, 125.05, 124.83, 119.17, 116.21, 72.87, 63.81, 35.57, 31.90, 31.62, 31.37, 30.45, 29.84, 29.45, 29.34, 29.28, 29.13, 14.11, 14.02. MALDI-TOF MS (m/z): [M] calcd. for $C_{100}H_{134}O_2S_4$, 1,494.93 $[M + H]^+$ found, 1,495.134.

IDTOT

$POCl_3$ (0.5 ml) was added to a solution of Compound 2 (400 mg, 0.27 mmol) in a mixed solvent of N,N-dimethylformamide

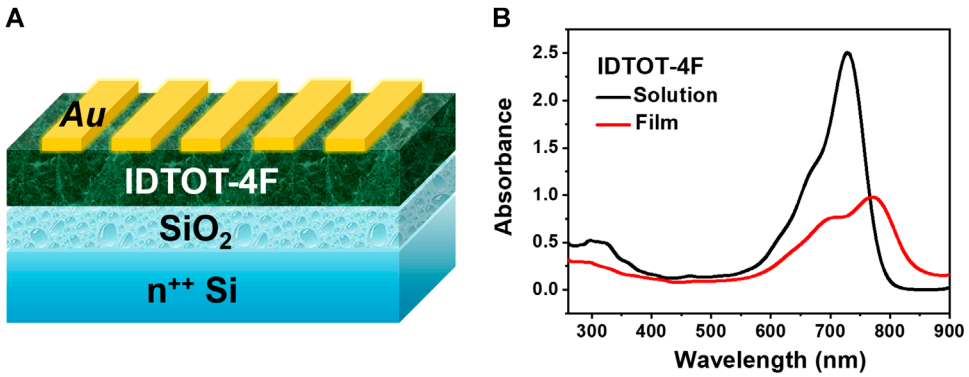

FIGURE 1 | (A) The structure of IDTOT-4F based optoelectrical devices; **(B)** The UV-vis absorption spectrum of IDTOT-4F in chloroform solution (concentration: 1.0×10^{-5} mol/L) and as thin film.

(DMF, 2.0 ml) and 1,2-dichloroethane (20 ml) at 0°C under nitrogen atmosphere. The mixture was stirred at this temperature for 1 h, then warmed to 80°C and reacted overnight. After cooling down to room temperature, the mixture was poured into ice water, neutralized with saturated Na_2CO_3 solutions, and extracted with dichloromethane. The combined organic phases were dried over anhydrous Na_2SO_4, filtered, and concentrated by reduced pressure. The resulting crude product was further purified by silica gel column chromatography (petroleum ether/dichloromethane = 1:2 v/v) to obtain an orange solid (377 mg, 90%). ^{1}H NMR (500M, $CDCl_3$, δ):9.96 (s, 2H), 7.30 (s, 2H), 7.23 (d, J = 8.2 Hz, 8H), 7.09 (s, 2H), 7.08 (d, J = 8.4 Hz, 8H), 3.23 (t, J = 7.2 Hz, 4H), 2.90 (t. J = 7.6 Hz, 4H), 2.57 (t, J = 7.6 Hz, 8H), 1.70–1.64 (m, 4H), 1.61–1.55 (m, 8H) overlapping 1.58 ($\underline{H_2}O$), 1.52–1.48 (m, 4H), 1.35–1.24 (m, 44H), 1.23–1.20 (m, 4H), 1.15–1.03 (m, 8H), 0.89–0.83 (m, 24H). ^{13}C (125M, $CDCl_3$, δ): 181.54, 155.69, 153.30, 151.40, 149.21, 144.44, 141.95, 140.58, 139.03, 135.24, 135.08, 130.55, 128.50, 128.28, 127.72, 125.94, 124.13, 116.71, 73.52, 63.98, 35.55, 31.85, 31.72, 31.53, 31.39, 31.35, 29.81, 29.37, 29.33, 29.19, 29.11, 28.46, 25.16, 22.65, 25.61, 14.10, 14.00. MALDI-TOF MS (m/z): [M] calcd. for $C_{102}H_{134}O_4S_4$, 1,550.92 $[M + H]^+$ found, 1,552.358.

IDTOT-4F

The electron-withdrawing end group 2-(5,6-difluoro-3-oxo-2,3-dihydro-1*H*-inden-1-ylidene)malononitrile (IC-2F) was synthesized following the reported literature (Yao et al., 2017). IDTOT (200 mg, 0.13 mmol) and IC-2F (89 mg, 0.39 mmol) were dissolved in a mixed solvent of pyridine (1 ml) and chloroform (25 ml). The mixture was deoxygenated with nitrogen for 10 min and then stirred at room temperature for 16 h. After poured the mixture into methanol (200 ml), the resulting precipitates were filtered and further purified by silica gel column chromatography (petroleum ether/dichloromethane = 1:1 v/v) to obtain a dark blue solid (210 mg, 82%). ^{1}H NMR (500M, $CDCl_3$, δ): 8.93 (s, 2H), 8.53–8.50 (m, 2H), 7.59 (t, J = 7.5 Hz, 2H), 7.37 (s, 2H), 7.27–7.25 (m, 10H) overlapping 7.26 ($C\underline{H}Cl_3$), 7.11 (d, J = 8.4 Hz, 8H), 3.35 (t, J = 7.1 Hz, 4H), 2.94 (t, J = 7.5 Hz, 4H), 2.59 (t, J = 7.6 Hz, 8H), 1.78–1.72 (m, 4H), 1.70–1.64 (m, 4H), 1.63–1.56 (m, 8H), 1.43–1.37 (m, 4H), 1.35–1.26 (m, 44H), 1.23–1.13 (m, 8H), 0.89–0.84 (m, 24H). ^{13}C (125M, $CDCl_3$, δ): 185.65, 162.28, 159.42, 156.54, 155.23, 153.80, 153.03, 144.25, 142.29, 138.54, 136.49, 136.43, 135.68, 134.55, 134.33, 131.66, 128.49, 128.45, 126.39, 118.90, 117.10, 115.20, 114.95, 114.81, 114.63, 112.25, 112.10, 74.22, 67.43, 64.09, 35.55, 31.87, 31.72, 31.62, 31.37, 30.02, 29.66, 29.42, 29.19, 29.10, 25.20,22.67, 22.61, 22.54, 14.11, 14.07. MALDI-TOF MS (m/z): [M] calcd. for $C_{126}H_{138}F_4N_4O_4S_4$, 1,974.95; $[M + H]^+$ found, 1,976.355.

Device Fabrication and Characterization

The structure of optoelectrical device is illustrated as **Figure 1A**. A solution of IDTOT-4F in *o*-dichlorobenzene (0.5 mg/ml) was drop casted on the pre-cleaned SiO_2/Si wafers, where the thickness of SiO_2 is approximate 300 nm with a capacitance of 11.5 nF/cm^2, and the thickness of the semiconductor layer is around 150 nm. Subsequently, the semiconductor layer was annealed at 120°C for 20 min and then transferred to the glove box. Finally, the source and drain electrodes of Au (50 nm) were thermally evaporated on the semiconductor layer through a shadow mask at a rate of 0.5 Å/sec. The channel width (W) is 5,600 μm and the channel length (L) is 200 μm. Electrical and photoresponse properties of IDTOT-4F-based devices were characterized by a Keithley (4200 SCS) semiconductor analyzer in air.

RESULTS AND DISCUSSION

Optical and Electrochemical Properties

According to the above-mentioned synthetic route (**Scheme 1**), IDTOT-4F was successfully synthesized with an A-π-D-π-A-type configuration, using indacenodithiophene as the central electron-donor (D) unit flanked with two thienyl units as the π-spacers and terminated with 2-(5,6-difluoro-3-oxo-2,3-dihydro-1*H*-inden-1-ylidene)malononitrile as the electron-acceptor (A) unit. Benefiting from the strong intramolecular charge transfer effect (Yao et al., 2017), IDTOT-4F in dilute chloroform

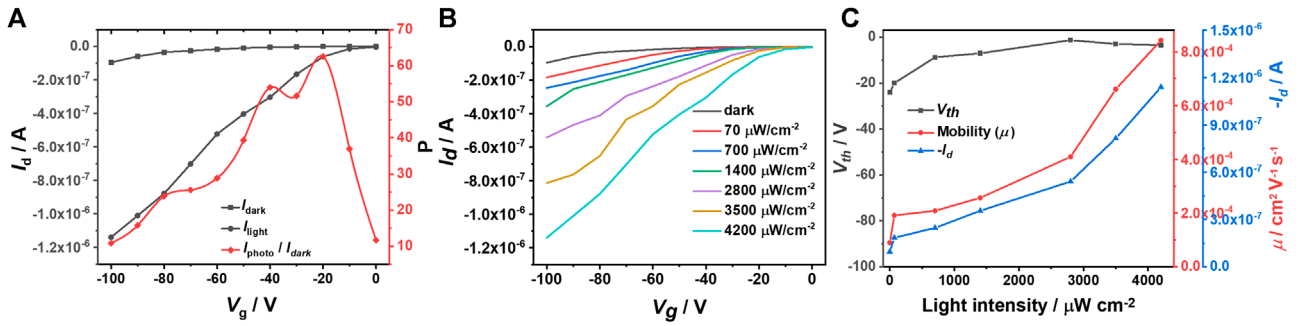

FIGURE 2 | (A) Transfer curves of (IDTOT-4F) based optoelectrical devices in the dark and under illumination, and the corresponding *P* values vs. V_g; **(B)** Transfer curves of optoelectrical devices at different light intensities with a constant pulse with of 10 sec; **(C)** Source-drain currents, threshold voltages (V_{th}) and mobilities (μ) vs. light intensities. The V_d values for the above measurements are set as −100 V.

solutions exhibits a broad and intense absorption band in the range of 550–800 nm with a maximum molar extinction coefficient (ε) of 2.51 × 10^5 M^{-1} cm^{-1}, as shown in **Figure 1B**. In going from solutions to films, the absorption maxima of IDTOT-4F shows a significant red-shift of 40 nm with an enhanced shoulder peak, indicating the formation of some molecular self-organization in the film (Lin et al., 2015). The optical bandgap of IDTOT-4F estimated from the absorption onset (850 nm) is 1.46 eV, following the equation $E_{g,opt}$ = 1,240/λ_{onset}. The oxidation and reduction onset potentials of IDTOT-4F are measured to be 0.87 and −0.85 V, respectively, through the electrochemical cyclic voltammetry characterization (Supplementary Figure S1). According to the equation $E_{HOMO/LUMO} = -e\,[E_{ox/red,onset} - E_{(Fc/Fc+)} + 4.80]$, where $E_{(Fc/Fc+)}$ is measured to be 0.14 V, the highest occupied molecular orbital and the lowest unoccupied molecular orbital energy levels of IDTOT-4F were calculated to be −5.53 and −3.81 eV, respectively.

Electrical Properties of Device

Considering IDTOT-4F possesses a high molar extinction coefficient and broad absorption band, which is beneficial for increasing photogenerated charge carriers during irradiation, we next study the electrical properties of its optoelectrical devices. In the dark, IDTOT-4F based devices exhibit both *n*-type and *p*-type switching behaviors. As shown in **Supplementary Figure S2**, the *n*-channel device obtains a saturated source-drain current (I_d) of around 50 nA and an electron mobility of 1.8 × 10^{-4} cm^2 V^{-1} sec^{-1} under vacuum at V_g = V_d = 100 V; and **Figure 2A** shows that the *p*-type channel device achieves an I_d of 96 nA and a hole mobility of 1.0 × 10^{-4} cm^2 V^{-1} sec^{-1} at V_g = V_d = − 100 V. Noticeably, when the *p*-type device is irradiated with white light (4,200 μW cm^{-2}) for 10 sec, the saturated I_d is significantly enhanced to 1.14 μA, with an increased hole mobility of 8.4 × 10^{-4} cm^2 V^{-1} sec^{-1} and a maximum *P* value (I_{photo}/I_{dark}) of 62 at V_g = − 20 V. Following the reported formulas (Han et al., 2019), the values of photoresponsivity (*R*) and detectivity (*D**) are almost positively correlated with gate voltage (**Supplementary Figure S3**), with maximum values of around 0.07 A W^{-1} and 2.5 × 10^{10} Jones, respectively, obtained at V_g = − 100 V. Subsequently, the influence of light intensity on IDTOD-4F based *p*-type optoelectrical devices is systematically investigated. The white light pulse width is 10 sec. As exhibited in **Figure 2B**, the source-drain current increases steadily as the light intensity increases from 0 to 4,200 μW cm^{-2} and the saturated I_d is positively correlated with light intensity (**Figure 2C**). The same trend is observed for the hole mobility, which rises from 9.0 × 10^{-5} to 8.4 × 10^{-4} cm^2 V^{-1} sec^{-1}. In addition, **Supplementary Figure S3** shows that *P* also increases as the light intensity increases, but *R* and *D** are less correlated with the light intensity. According to equation $R = I_{photo}/(p \times A)$, where *p* is the light intensity and *A* is the area of the semiconductor on the channel of device, I_{photo}/p should be a constant because I_{photo} shows a good linear relationship with light intensity (**Figure 2C**); therefore, *R* should be a constant and there exists no clear relationship between *R* (and corresponding *D**) and the light intensity.

Apart from the light intensity, the light pulse width could also improve the saturated I_d due to the formation of more photogenerated charge carriers in the channel with longer irradiation time. **Figure 3** indicates that the saturated I_d and the hole mobility increase linearly with the pulse width at a constant light intensity of 700 μW cm^{-2}. Noticeably, here *p* and *A* are constants, and therefore, according to equation $R = I_{photo}/(p \times A)$, *R* should be positively correlated with I_{photo} that means extending the pulse width could improve *p*, *R* and *D** values simultaneously, as shown in **Supplementary Figure S4**. Additionally, IDTOT-4F based optoelectrical devices exhibit obvious bias stress behavior. As shown in **Supplementary Figure S5A**, the saturated I_d drops dramatically when the device is measured continuously (every 30 sec). Fortunately, the resilience of these devices is good and **Supplementary Figure S5B** shows that the saturated I_d could reach the initial value when the device is measured every 5 min. Therefore, the above-mentioned measurements with different light intensity and pulse width are conducted every 5 min.

Optical Memory Characteristics

Surprisingly, we notice that this semiconductor exhibits good optical memory behavior. As shown in **Figure 4A**, we measure

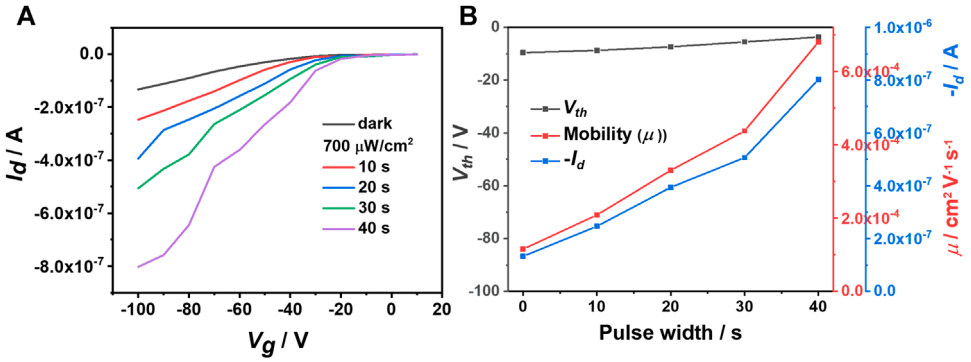

FIGURE 3 | (A) Transfer curves of IDTOT-4F based optoelectrical devices under illumination with different pulse widths (V_d = −100 V); **(B)** Source-drain currents, threshold voltages (V_{th}) and mobilities (μ) vs. light pulse widths.

transfer curves of IDTOT-4F based *p*-type optoelectrical devices at different retention time ($V_g = V_d = -100$ V). The initially saturated I_d value of the optoelectrical device under dark conditions is 133 nA. Once the device is irradiated at 4,200 μW cm^{-2} for 1 min, the saturated I_d value is dramatically improved to 1.67 μA. It is worth noting that after keeping the device in the dark for 24 h, the saturated I_d value still maintains over 800 nA, which is much higher than the initial value (133 nA). Even after 44 h, the device still shows some optical memory behaviors with the saturated I_d value around 222 nA. Biexponential fitting of the current decay curve gives τ_1 of 4.6 h and τ_2 of 14,842.4 h (**Supplementary Figure S6**). In order to verify the optical memory nature of IDTOT-4F based optoelectrical devices, we conduct a blank control experiment with the device measured in the dark during the whole time (**Supplementary Figure S7A**). The saturated I_d value drops from the initial 145 to 84 nA after 24 h. As shown in **Figure 4B**, comparing the retention characteristics between the dark current and the photocurrent, it is found that IDTOT-4F based optoelectrical devices possess good optical memory ability. Another control experiment with P3HT as the semiconducting layer provides further evidence for the good optical memory behavior of IDTOT-4F (**Supplementary Figure S7B**). The optical memory behavior of IDTOT-4F is presumably elucidated as following: under dark conditions, some holes induced by the gate voltage are trapped at the IDTOT-4F/SiO_2 interface, thus suppressing the current. Upon illumination, beneficial from the strong light-absorbing and broad absorption band of IDTOT-4F, the devices gain a lot of photogenerated excitons, which could be dissociated into carriers very fast driven by the large drain voltage. Under the lateral electric field, the separated electron and hole would accumulate at source/drain electrodes, respectively, leading to band bending at semiconductor surfaces and lowering the potential barrier for hole injection. Consequently, more holes are injected into the channel, together with photogenerated holes, the I_d are significantly promoted. Further, because of the low intrinsic hole mobility (less than 10^{-3} cm^2 V^{-1} sec^{-1}) of IDTOT-4F, the photogenerated carriers could not be injected into the channel in a timely manner and therefore a certain number of photogenerated carriers still remain in the semiconductor layer. The minority carriers recombine slowly and could persist for a long time, thus slowing the recovery of current and prolonging the optical memory time.

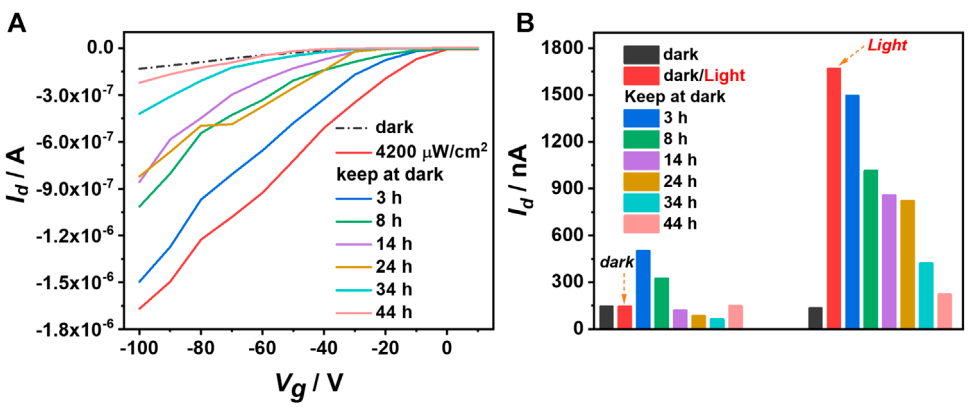

FIGURE 4 | (A) Transfer curves of the photocurrent retention characteristics for IDTOT-4F based optoelectrical devices (V_d = −100 V); **(B)** Histogram contrast between the memory behaviors of the dark current and the photocurrent.

CONCLUSION

In conclusion, we synthesize a novel A-π-D-π-A-type organic semiconductor named as IDTOT-4F. Benefiting from the strong intramolecular charge transfer effect, IDTOT-4F possesses a broad absorption band ranging from 550 to 850 nm, a narrow bandgap of 1.46 eV, and a high molar extinction coefficient of $2.51 \times 10^5\ M^{-1}\ cm^{-1}$. The optoelectrical devices based on IDTOT-4F exhibit both *n*-type and *p*-type switching behaviors. Noticeably, the *p*-channel devices based on IDTOT-4F exhibit good photoresponse properties. Upon white light irradiation ($4{,}200\ \mu W\ cm^{-2}$) for 10 sec, the *p*-type device achieves a saturated I_d of 1.14 μA ($V_g = V_d = -100$ V) with *P*, *R* and D^* values of around 60, 0.07 A W^{-1} and 2.5×10^{10} Jones, respectively. The light intensity and pulse width could promote the photogenerated charge carriers, thus leading to enhanced photoresponsive behaviors and higher hole mobilities. More importantly, IDTOT-4F based optoelectrical devices exhibit good optical memory characteristics and biexponential fitting of the current decay curve gives τ_1 of 4.6 h, indicating its applicability to nonvolatile optical memory devices. The results provide new insights into the photoresponsive behavior of fused-ring semiconductors and pave the way for the design of nonvolatile optical memory devices.

DATA AVAILABILITY STATEMENT

The raw data supporting the conclusions of this article will be made available by the authors, without undue reservation.

AUTHOR CONTRIBUTIONS

SF performed the experiments and wrote the manuscript. WH directed the project. All authors contributed to the data analyses.

ACKNOWLEDGMENTS

This work was supported by the start-up funding from FJIRSM-CAS, and National Natural Science foundation of China (51803214). WH is also grateful for the award of "The Recruitment Program of Global Youth Experts."

SUPPLEMENTARY MATERIAL

The Supplementary Material for this article can be found online at: https://www.frontiersin.org/articles/10.3389/fmats.2020.567031/full#supplementary-material

REFERENCES

Cheng, S.-W., Han, T., Huang, T.-Y., Chang Chien, Y.-H., Liu, C.-L., Tang, B. Z., et al. (2018). Novel organic phototransistor-based nonvolatile memory integrated with UV-sensing/green-emissive aggregation enhanced emission (AEE)-active aromatic polyamide electret layer. *ACS Appl. Mater. Interfaces* 10, 18281–18288. doi:10.1021/acsami.8b02560

Dai, S., Zhao, Y., Wang, Y., Zhang, J., Fang, L., Jin, S., et al. (2019). Recent advances in transistor-based artificial synapses. *Adv. Funct. Mater.* 29, 1903700. doi:10.1002/adfm.201903700

de Arquer, F. P. G., Armin, A., Meredith, P., and Sargent, E. H. (2017). Solution-processed semiconductors for next-generation photodetectors. *Nat. Rev. Mater.* 2, 16100. doi:10.1038/natrevmats.2016.100

Deng, W., Zhang, X., Jia, R., Huang, L., Zhang, X., and Jie, J., (2019). Organic molecular crystal-based photosynaptic devices for an artificial visual-perception system. *NPG Asia Mater.* 11, 77. doi:10.1038/s41427-019-0182-2

Han, T., Shou, M., Liu, L., Xie, Z., Ying, L., Jiang, C., et al. (2019). Ultrahigh photosensitive organic phototransistors by photoelectric dual control. *J. Mater. Chem. C* 7, 4725–4732. doi:10.1039/c9tc00324j

Hou, J., Inganäs, O., Friend, R. H., and Gao, F. (2018). Organic solar cells based on non-fullerene acceptors. *Nat. Mater.* 17, 119–128. doi:10.1038/nmat5063

Huang, J., Lee, J., Vollbrecht, J., Brus, V. V., Dixon, A. L., Cao, D. X., et al. (2020). A high-performance solution-processed organic photodetector for near-infrared sensing. *Adv. Mater.* 32, 1906027. doi:10.1002/adma.201906027

Lee, J., Ko, S.-J., Lee, H., Huang, J., Zhu, Z., Seifrid, M., et al. (2019). Side-chain engineering of nonfullerene acceptors for near-infrared organic photodetectors and photovoltaics. *ACS Energy Lett.* 4, 1401–1409. doi:10.1021/acsenergylett.9b00721

Leydecker, T., Herder, M., Pavlica, E., Bratina, G., Hecht, S., Orgiu, E., et al. (2016). Flexible non-volatile optical memory thin-film transistor device with over 256 distinct levels based on an organic bicomponent blend. *Nat. Nanotechnol.* 11, 769–775. doi:10.1038/nnano.2016.87

Li, M., Liu, Y., Zhou, Y., Yang, L., Shen, S., Song, J., et al. (2020). Photovoltaic performances of fused ring acceptors with isomerized ladder-type dipyran cores. *ACS Appl. Mater. Interfaces* 12, 4887–4894. doi:10.1021/acsami.9b19676

Li, W., Xu, Y., Meng, X., Xiao, Z., Li, R., Jiang, L., et al. (2019). Visible to near-infrared photodetection based on ternary organic heterojunctions. *Adv. Funct. Mater.* 29, 1808948. doi:10.1002/adfm.201808948

Lin, Y., Wang, J., Zhang, Z.-G., Bai, H., Li, Y., Zhu, D., et al. (2015). An electron acceptor challenging fullerenes for efficient polymer solar cells. *Adv. Mater.* 27, 1170–1174. doi:10.1002/adma.201404317

Liu, Y., Li, M., Zhou, X., Jia, Q.-Q., Feng, S., Jiang, P., et al. (2018). Nonfullerene acceptors with enhanced solubility and ordered packing for high-efficiency polymer solar cells. *ACS Energy Lett.* 3, 1832–1839. doi:10.1021/acsenergylett.8b00928.

Liu, Y., Yang, Y., Shi, D., Xiao, M., Jiang, L., Tian, J., et al. (2019). Photo-/thermal-responsive field-effect transistor upon blending polymeric semiconductor with hexaarylbiimidazole toward photonically programmable and thermally erasable memory device. *Adv. Mater.* 31, 1902576. doi:10.1002/adma.201902576

Park, S., Fukuda, K., Wang, M., Lee, C., Yokota, T., Jin, H., et al. (2018). Ultraflexible near-infrared organic photodetectors for conformal photoplethysmogram sensors. *Adv. Mater.* 30, 1802359. doi:10.1002/adma.201802359

Park, Y., and Lee, J.-S. (2017). Artificial synapses with short- and long-term memory for spiking neural networks based on renewable materials. *ACS Nano* 11, 8962–8969. doi:10.1021/acsnano.7b03347

Shi, W., Guo, Y., and Liu, Y. (2020). When flexible organic field-effect transistors meet biomimetics: a prospective view of the internet of things. *Adv. Mater.* 32, 1901493. doi:10.1002/adma.201901493

Yan, C., Barlow, S., Wang, Z., Yan, H., Jen, A. K.-Y., Marder, S. R., et al. (2018). Non-fullerene acceptors for organic solar cells. *Nat. Rev. Mater.* 3, 18003. doi:10.1038/natrevmats.2018.3

Yao, H., Cui, Y., Yu, R., Gao, B., Zhang, H., and Hou, J. (2017). Design, synthesis, and photovoltaic characterization of a small molecular acceptor with an ultra-narrow band gap. *Angew. Chem. Int. Ed.* 56, 3045–3049. doi:10.1002/anie.201610944

Yu, Y., Ma, Q., Ling, H., Li, W., Ju, R., Bian, L., et al. (2019). Small-molecule-based organic field-effect transistor for nonvolatile memory and artificial synapse. *Adv. Funct. Mater.* 29, 1904602. doi:10.1002/adfm.201904602

Conflict of Interest: The authors declare that the research was conducted in the absence of any commercial or financial relationships that could be construed as a potential conflict of interest.